

FEDSM-ICNMM2010-3\$\$(&

TWO-DEGREE-OF-FREEDOM FLOW-INDUCED VIBRATIONS OF A CIRCULAR CYLINDER WITH A HIGH MOMENT OF INERTIA RATIO

Sina Kheirkhah
University of Waterloo
Waterloo, Ontario, Canada

Serhiy Yarusevych
University of Waterloo
Waterloo, Ontario, Canada

ABSTRACT

Two degree-of-freedom vortex-induced vibrations of a moderate mass and high moment of inertia ratio pivoted cylinder were investigated experimentally. The experiments were performed at a constant Reynolds number of 2100 for a range of reduced velocities from 3.4 to 11.25. The results show that, in addition to the reduced velocity, the transverse damping ratio has a significant effect on the amplitudes of response. The cylinder tip is observed to trace orbital trajectories, which is shown to be attributed to the frequencies of oscillations in both directions locking onto the natural frequency in the synchronization region. The results indicate that a phase angle between the streamwise and transverse oscillations governs the direction and orientation of the orbiting motion. Flow visualization results show that, at a given reduced velocity and transverse damping ratio, near-wake development changes along the cylinder span. The observed shedding patterns are shown to differ from those expected at the corresponding experimental parameters for one-degree-of-freedom uniform amplitude cylinder vibrations.

1. INTRODUCTION

Vortex-induced vibrations (VIV) of cylindrical structures are important in many engineering applications, e.g., in civil and offshore structures. Amplitudes of these vibrations can increase up to 2.5 cylinder diameters and may result in structural failures [1-3]. Through the past several decades, most of the VIV investigations of cylindrical structures have been performed for uniform, circular cylinders with one-degree-of-freedom (one DOF), i.e., the ability to vibrate transverse to the flow [4-9]. These investigations have shown that amplitudes of vortex-induced vibrations of low mass damping ratio cylinders ($m^*\zeta_Y \sim 0.01$) exhibit a three-branch type of response, featuring initial, upper, and lower branches [8-11]. The transition from

the initial branch to the upper branch is hysteretic and that from the upper branch to the lower branch is intermittent [8-11]. In contrast, for high mass damping ratio cylinders ($m^*\zeta_Y \sim 1$), a two-branch type of amplitude response has been observed [4], with a hysteretic transition between the initial and lower branches. Previous studies have shown a clear link between the amplitude response and wake flow development [11-13]. For the initial branch of response, two single vortices form in the wake per cycle of oscillation, often referred to as a 2S vortex shedding pattern. On the other hand, for both the upper and lower branches of response, two pairs of vortices form per cycle of oscillation, referred to as a 2P vortex shedding pattern. Other possible vortex shedding patterns associated with the vortex-induced vibrations of the uniform cylinders have been investigated using controlled oscillations, e.g., [12 and 13], with the results compiled into a well-known Williamson-Roshko map [12] and updated in subsequent studies, e.g., [13].

Detailed reviews of studies focused on one DOF VIV of uniform circular cylinders can be found, for example, in [11, 14 and 15]. Although such studies provide invaluable insight into VIV of cylindrical structures, when the cylinder is allowed to vibrate streamwise as well as transverse the flow, different amplitude response and wake vortex shedding patterns can occur [16-21]. For example, the results of Jauvtis and Williamson [16] suggest that the transverse and streamwise amplitudes of response of a two DOF cylinder [16] exhibit the three-branch type of response, with a “supper-upper” branch replacing the upper branch for low mass damping ratios and mass ratios of less than 6. Similar to one DOF studies, the results in [16] show that the initial and lower branches of amplitude response of two DOF uniform cylinders are associated with 2S and 2P patterns, respectively. However, the supper-upper branch of response is associated with the formation of three vortices per half cycle of oscillation, termed

a 2T vortex shedding pattern in [16]. It should be noted that for the VIV of their “two-independent-axes” traversing setup, Jeon and Gharib [17] observed a 2S vortex shedding pattern, rather than 2P, for the lower branch of response.

The results of previous two DOF VIV investigations of low mass ratio circular cylinders show that the streamwise frequency of oscillations is about twice that of the transverse oscillations [16, 20], with the corresponding vibration amplitudes given by Eqs. 1a and b. Therefore, the cylinders trace Lissajous-type trajectories.

$$Y/D = A_Y^* \sin(2\pi f_{os,Y} t) \quad (1a)$$

$$X/D = A_X^* \sin(4\pi f_{os,Y} t + \theta) \quad (1b)$$

Adding the freedom of the uniform circular cylinders to vibrate streamwise as well as transverse to the flow serves to create a more realistic model of VIV occurring in practical engineering applications [16-18]. However, in most applications, the streamwise and transverse amplitudes of response vary along the span of the structure [1]. Recently, a few studies investigated the effect of spanwise amplitude variation on VIV using rigid, pivoted models, representing two DOF models with linear variation of vibration amplitude along the span [22, 23]. These studies show that such structures may exhibit different response compared to that observed for two DOF cylinders undergoing uniform amplitude VIV. Also, it was observed that vortex shedding patterns may vary along the span [22, 23]. For a low mass and moment of inertia ratio pendulum-like pivoted cylinder, Flemming and Williamson [22] observed a three-branch type of response, in which the upper and lower branches intersect on the amplitude of response plot. They showed that the vortex shedding pattern at a given spanwise location agrees with that expected from Williamson-Roshko map based on the local transverse amplitude of vibrations. The formation of two co-rotating vortices, termed a 2C pattern in [22], was observed for the upper branch of response. For a very low mass ratio pivoted cylinder mounted as an inverted pendulum, Leong and Wei [23] reported only two branches of response, initial and upper branches. Their results show that the initial branch is associated with a 2S pattern of shedding, while the upper branch is linked either to a 2P pattern or a P+S pattern (i.e., the formation of a pair of vortices and a single vortex per cycle of oscillation). Similar to the case of uniform amplitude VIV, it has been shown in [22] and [23] that the streamwise frequency of vibrations is about twice that of the transverse oscillation for pivoted low mass and moment of inertia ratio cylinders. Therefore, the cylinders have been observed to trace Lissajous-type trajectories.

To date, the investigations of vortex-induced vibrations of two DOF circular cylinders with linear amplitude of vibrations have been performed only for cylinders with moment of inertia ratios less than 8 (Table 1). Since the moment of inertia ratio can significantly influence the VIV of pivoted cylinders, this study is aimed at investigating the VIV of a high moment of inertia ratio pivoted circular cylinder. Also, previous

investigations were conducted at a fixed mass damping ratio. By performing experiments at a constant Reynolds number and a range of $m^* \zeta_Y$, the effect of transverse damping ratio is investigated in the present study.

Investigators	m^*	I^*	$m^* \zeta_Y$	U^*	Re
Leong & Wei [23]	0.45	1.41 [†]	0.026	1.1-8.3	820-6050
Flemming & Williamson, [22]	1.03, 2.68, 7.69	1.03, 2.68, 7.69	0.032	2.8-20.2	340-2600
Present Study	17.6	72	0.014-0.12	3.4-11.3	2100

Table 1. VIV INVESTIGATIONS OF PIVOTED CYLINDERS. [†]THE NUMBER IS ESTIMATED BY THE AUTHORS BASED ON THE RELEVANT PARAMETERS PRESENTED IN [23].

NOMENCLATURE

A_X	=	streamwise amplitude of vibrations
A_X^*	=	normalized streamwise amplitude of vibrations, A_X / D
A_Y	=	transverse amplitude of vibrations
A_Y^*	=	normalized transverse amplitude of vibrations, A_Y / D
D	=	cylinder diameter
f_n	=	natural frequency in still water
$f_{os,X}$	=	frequency of streamwise vibrations
$f_{os,X}^*$	=	normalized frequency of streamwise vibrations, $f_{os,X} / f_n$
$f_{os,Y}$	=	frequency of transverse vibrations
$f_{os,Y}^*$	=	normalized frequency of transverse vibrations, $f_{os,Y} / f_n$
f_{st}	=	Strouhal frequency
i	=	$\sqrt{-1}$
I	=	moment of inertia of the pivoted cylinder about the contact point
I_d	=	moment of inertia of the displaced fluid
I^*	=	moment of inertia ratio, I / I_d
L	=	length of the cylinder
m	=	mass of the structure

m_d	=	mass of displaced fluid
m^*	=	mass ratio, m/m_d
$m^* \zeta_Y$	=	mass damping ratio
PSD	=	normalized power spectrum density
Re	=	Reynolds number, UD/ν
St	=	Strouhal number, $f_{st}D/U$
U	=	free-stream velocity
U^*	=	reduced velocity, $U/f_n D$
$X(t)$	=	streamwise vibrations
$Y(t)$	=	transverse vibrations
ζ_Y	=	transverse damping ratio
θ	=	phase angle between the transverse and streamwise vibrations
λ^*	=	normalized wave length
ν	=	kinematic viscosity

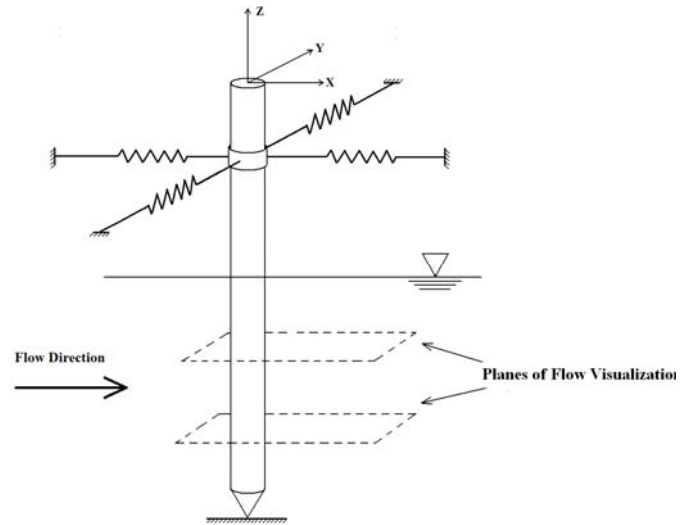


FIG. 1 EXPERIMENTAL SETUP.

2. EXPERIMENTAL SETUP

All of the experiments were performed in a water flume facility at the University of Waterloo. The test section of the flume has a 120 cm \times 120 cm cross section. In this study, the water level in the test section was maintained at 80 cm. The experiments were performed at a free-stream velocity (U) of 87 mm/s, with the attendant free-stream turbulence intensity of less than 1%.

A steel circular cylinder was placed in the water flume as an inverted pendulum (Fig. 1). The cylinder had a diameter (D) of 25.4 mm, a length (L) of 1.64 m, a mass (m) of 6.8 Kg, and a moment of inertia about the contact point (I) of 6.4 Kg \times m². One end of the cylinder was tapered in order to provide a low-friction contact point at the bottom of the flume. The cylinder was supported with two pairs of springs of the same stiffness (Fig. 1), one pair aligned parallel to and the other orthogonal to the flow direction. Within the uncertainty of less than 2%, the natural frequency of the structure in the streamwise direction was equal to that in the transverse direction for all cases examined. Since the free-stream velocity was maintained constant throughout the experiments to eliminate any Reynolds number effects, the reduced velocity (U^*) was varied by varying the natural frequency of the structure (f_n). Three different springs (24.5, 35, and 79.9 N/m) were used throughout the experiments. By changing the stiffness and/or the spanwise location of the springs, the natural frequency of the structure was varied between 0.31 and 1 Hz, corresponding to $3.4 \leq U^* \leq 11.25$. The natural frequency of the structure was determined via the spectral analysis of the free vibration measurements in still water.

The transverse damping ratio (ζ_Y) of one DOF structures is usually estimated based on the amplitude decay of free vibrations in air, e.g., [8] (Fig 2a). Similar approach can be used for two DOF experimental setups that allow uncoupled free vibration tests in the transverse and the streamwise directions, e.g., [18, 21]. However, the experimental setup employed in this study undergoes coupled two DOF free vibrations, similar to those observed in most engineering structures. In this case, the amplitude decay is characterized by a bi-exponential curve fit (Fig. 2b), agreeing with the results reported for two DOF systems [24]. Therefore, the transverse damping ratio of a two DOF structure is a function of the transverse amplitude of vibrations. Thus, for a given U^* , the transverse damping ratio was estimated based on a data segment of free vibration amplitude decay measurements (Fig. 2b) corresponding to the transverse amplitude of in-flow vibrations of the structure.

Two laser-based displacement sensors were used to measure the transverse and streamwise oscillations of the cylinder. The uncertainty of the displacement measurements is estimated to be within $\pm 0.004 D$. Laser-Induced-Fluorescence (LIF) was used to visualize flow development in the cylinder wake at two different elevations along the span, $Z/L = -0.65$ and $Z/L = -0.84$ (Fig. 1). A stationary probe located 1D upstream of the cylinder was used to inject fluorescent dye into the flow. The dye was illuminated with a laser sheet and the flow visualization images were acquired at an average rate of 6 frames per second using a digital camera. Also, video recordings were made to allow a more detailed analysis of vortex shedding patterns.

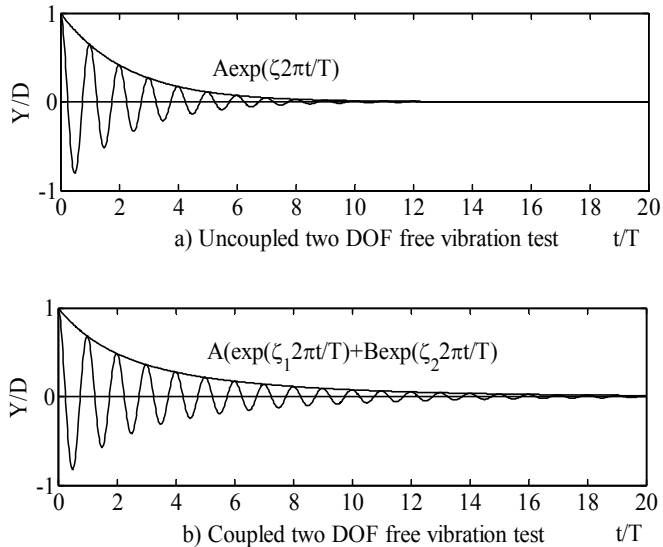


FIG. 2 TYPICAL AMPLITUDE DECAY OF FREE VIBRATIONS IN AIR.

3. RESULTS

All experimental results presented correspond to $Re=2100$. The results are grouped into three sections. First, the amplitudes of response and the effect of the transverse damping ratio are discussed. Then, frequencies and trajectories of the vibrating structure are presented. Finally, wake vortex shedding patterns are analyzed based on flow visualization images.

3.1 Amplitudes of response

Figure 3 shows the variation of transverse amplitude of response with reduced velocity. It should be noted that the amplitudes of response are defined as half of peak to peak amplitudes of the cylinder tip undergoing steady-state oscillations. For a constant spring stiffness, e.g. $k=35$ N/m, the amplitude of response increases as the reduced velocity increases, peaking at $U^*=5.7$. Further increase of the reduced velocity, results in amplitude decrease. Flemming and Williamson [22] report a similar trend. However, for a pivoted cylinder with a mass ratio less than 0.54, Leong and Wei [23] observed that the amplitude remains nearly constant within the lock-in region for about $U^* > 4.4$. Also, in comparison with the results reported in [22], the hysteretic behavior was not observed for the amplitude of response in the present study. As discussed in [8], the hysteretic behavior occurs when U^* is varied by adjusting the free-stream velocity. However, in the present investigation, the free-stream velocity was kept constant throughout all of the experiments.

The results in Fig. 3 show that, at a given U^* , different amplitudes can be attained by varying spring stiffness. For the structure investigated, a dimensional analysis can be used to show that the amplitudes of response (A_y^* and A_x^*) depend on the Reynolds number, the reduced velocity, and the transverse damping ratio. Since the experiments were performed at a constant Reynolds number, it can be concluded that the

observed difference between the amplitudes of response at a given reduced velocity (Fig. 3), is due to the difference in the transverse damping ratios. Consequently, the amplitude response should be presented on three dimensional plots, as shown in Figs. 4 and 5. The results illustrate that the transverse damping ratio is indeed an important governing parameter that has a considerable effect on the amplitudes of vibrations, agreeing with Sarpkaya [15] and Blevins and Coughran [19]. For example, a comparison of the amplitudes of response at $U^*=6.6$ shows that decreasing the transverse damping ratio by about 30% results in the transverse and streamwise amplitudes increasing by about 35% and 90%, respectively. Thus, for a constant Reynolds number, the amplitude of response, is in fact a surface, whose shape depends on the reduced velocity and the transverse damping ratio.

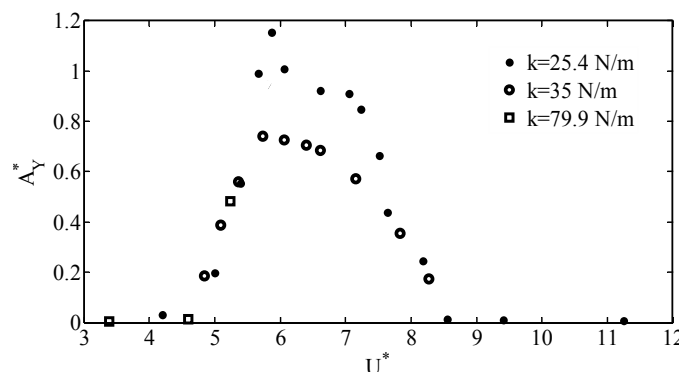


FIG. 3 TRANSVERSE AMPLITUDE OF RESPONSE VERSUS REDUCED VELOCITY.

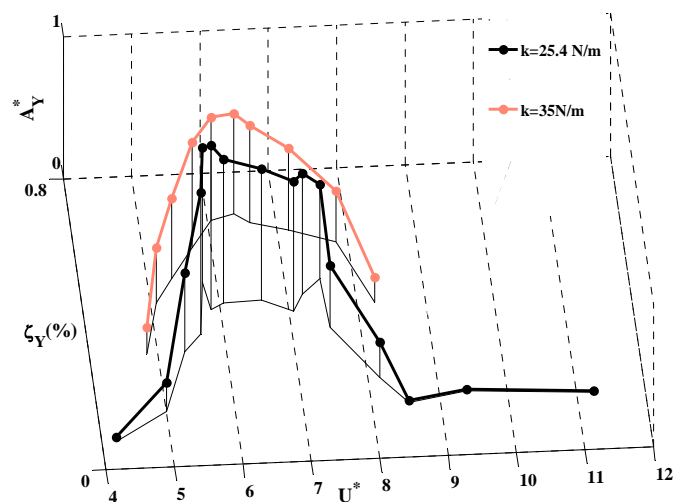


FIG. 4 TRANSVERSE AMPLITUDES OF VIBRATIONS VERSUS REDUCED VELOCITY AND TRANSVERSE DAMPING RATIO.

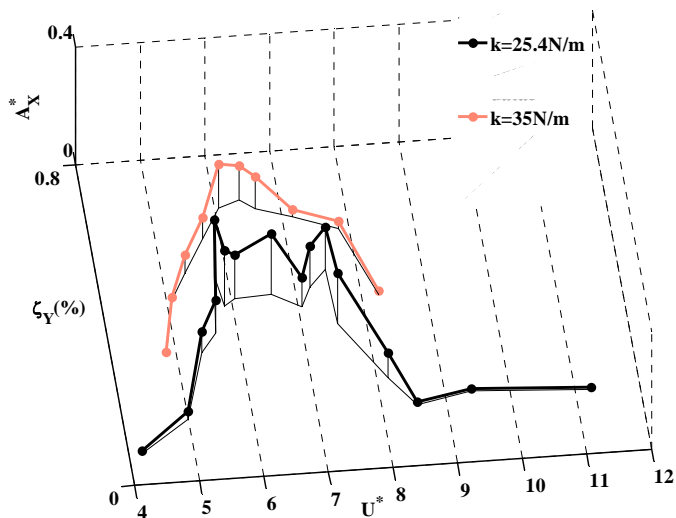


FIG. 5 STREAMWISE AMPLITUDES OF VIBRATIONS VERSUS REDUCED VELOCITY AND TRANSVERSE DAMPING RATIO.

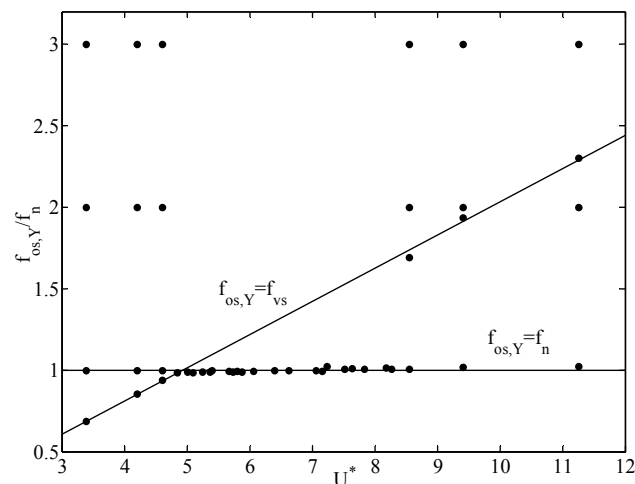


FIG. 6 FREQUENCY OF TRANSVERSE VIBRATIONS.

3.2 Frequencies and trajectories of response

Figure 6 shows the variation of the normalized frequency of transverse vibrations ($f_{os,Y}^*$) with the reduced velocity. The frequencies were obtained via spectral analysis of vibrations, with spectra at selected reduced velocities presented in Fig. 7. In Fig. 6, distinct regions of frequency response can be identified based on the number of peaks in the corresponding spectra. For $4.85 < U^* < 8.55$, the spectra of transverse vibrations, depicted in Fig. 7a, show a single peak at the natural frequency, similar to the frequency of response presented by Flemming and Williamson [22]. For $3.4 < U^* < 4.85$ and $8.55 < U^* < 11.25$, the corresponding spectra of transverse vibrations, e.g. 7b and 7c, display peaks centered at the Strouhal frequency, the natural frequency, and the harmonics of the natural frequency. Similar frequency response behavior is reported for $3.4 < U^* < 4.85$ in [22]. However, for $8.55 < U^* < 11.25$, Flemming and Williamson [22] observed that $f_{os,Y}$ does not lock onto the Strouhal frequency or the natural frequency. Leong and Wei [23], who report $f_{os,Y}$ locking onto the Strouhal frequency within $3.4 < U^* < 4.85$ and $8.55 < U^* < 11.25$, suggest that the discrepancies between their results and those from [22] are attributed to the differences in mass ratios investigated. Indeed, there is also a significant difference between the mass ratios studied in [22] and [23] and that investigated here (Table 1).

The frequency response of streamwise vibrations is shown in Fig. 8. The results suggest that the normalized frequency of streamwise vibrations is equal to the natural frequency of the structure for the range of reduced velocities investigated. Since the frequencies of both the streamwise and transverse vibrations of the cylinder lock onto the natural frequency for $4.85 < U^* < 8.55$, the vibrations can be represented by Eqs. 2a and 2b.

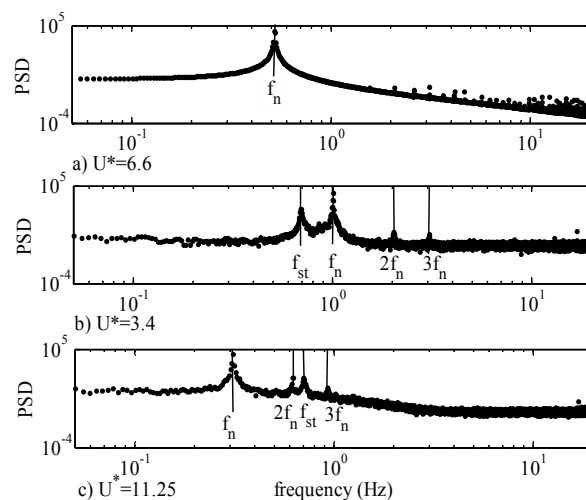


FIG. 7 SPECTRA OF TRANSVERSE VIBRATIONS.

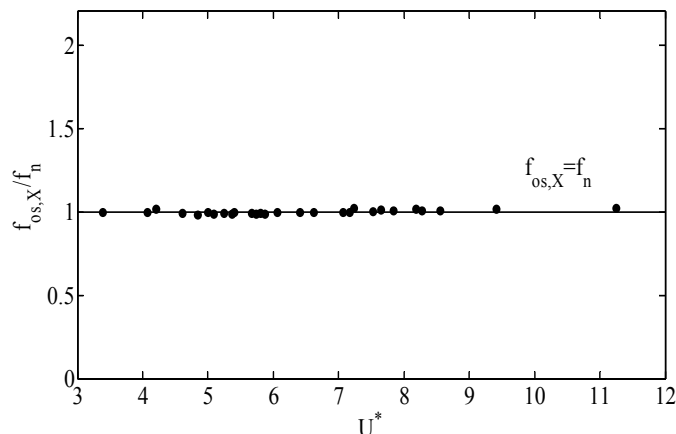


FIG. 8 FREQUENCY OF STREAMWISE VIBRATIONS

$$Y/D = A_Y^* \sin(2\pi f_n t) \quad (2a)$$

$$X/D = A_X^* \sin(2\pi f_n t + \theta) \quad (2b)$$

Using Eqs. 2, possible cylinder trajectories were predicted for a range of phase angles (θ). The results shown in Fig. 9 predict orbiting motion for the cylinder.

Figures 10a and b depict two experimentally obtained trajectories for $U^*=6.6$ and $\zeta_Y=0.45\%$, and for $U^*=6.6$ and $\zeta_Y=0.66\%$, respectively. The results show that the structure undergoes orbiting motion, similar to the predicted trajectories in Fig. 9. Also, it can be seen that the transverse damping ratio can affect the orientation of the trajectories, which is linked to the changes in the phase angle (Fig. 9). The observed structural response, different from Lisajous-type trajectories reported in [22] and [23], but reported to occur in cylindrical structures [25, 26] may be attributed to the moment of inertia ratio of the structure being significantly higher than that investigated in [22] and [23] and/or to a coupling between the reactions of the streamwise and transverse springs

In comparison with the trajectories observed for $4.85 < U^* < 8.55$, the cylinder undergoes irregular, low amplitude vibrations for $3.5 < U^* < 4.85$ and $8.55 < U^* < 11.25$.

To estimate the phase angle between the streamwise and the transverse vibrations of the structure, the Hilbert transform was utilized. The Hilbert transform of a signal $x(t)$ is given by Eq. 3a. The phase of a signal $x(t)$ is equal to the phase of a complex function $z(t)$ given by Eq. 3b.

$$H(x) = \frac{1}{\pi} \int_{-\infty}^{\infty} \frac{x(t)}{t-s} dt \quad (3a)$$

$$z(t) = x(t) - iH[x(t)] \quad (3b)$$

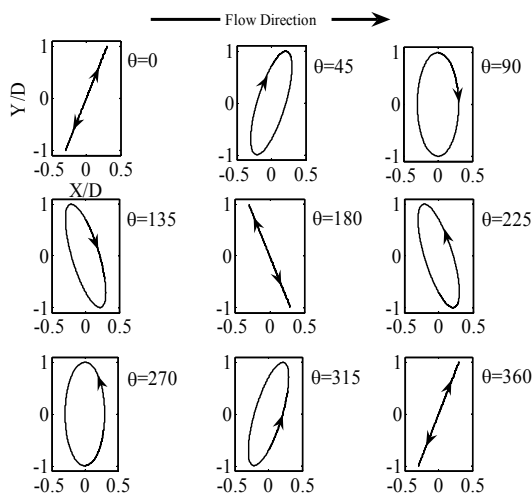


FIG. 9 POSSIBLE CYLINDER TRAJECTORIES.

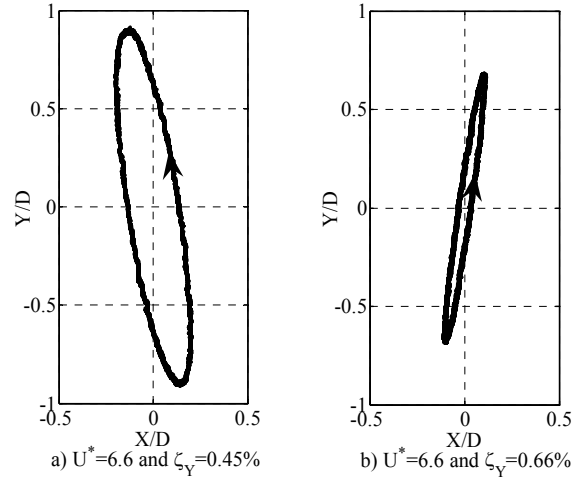


FIG. 10 CYLINDER TIP TRAJECTORIES FOR 50 CYCLES.

The phase angle variations in time for the test cases shown in Figs. 10a and b are plotted in Figs. 11a and b, respectively. The results show that the phase angle remains nearly constant with time for these two cases, both corresponding to the synchronization region. From Figs. 11a and b, the phase angles for the trajectories shown in Figs. 10a and b are $\theta=225.2^\circ$ and $\theta=342.2^\circ$, respectively. Thus, the experimentally measured trajectories (Fig. 10a and b) agree with those expected based on the Eqs. 2 for the corresponding phase angles (Fig. 9). Fig. 11c shows the variation of the phase angle with time for $U^*=11.25$ and $\zeta_Y=0.16\%$. The random fluctuations in θ presented in Fig. 11c are associated with the irregular, low amplitude vibrations of the structure.

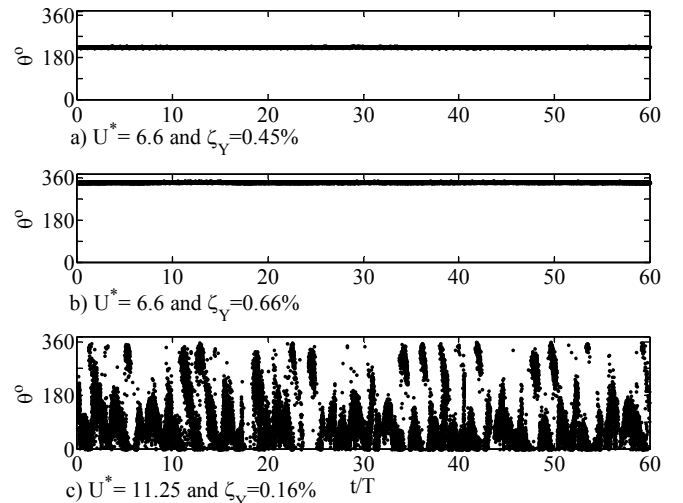


FIG. 11 TIME VARIATION OF THE PHASE ANGLE FOR THE SYNCHRONIZED (A AND B) AND NON-SYNCHRONIZED VIBRATIONS (C).

3.3 Vortex shedding in the cylinder wake

The results discussed in previous sections show that the reduced velocity and the transverse damping ratio govern the structural response. Thus, these two parameters are expected to influence the wake development. Here, the effect of the transverse damping ratio on the wake vortex pattern as well as the variation of the vortex pattern along the span are investigated. A comparative analysis is carried out for flow visualization results obtained at $U^*=6.6$, and a summary of the experimental conditions is presented in Table 2. The two selected transverse damping ratios were chosen because they produce distinctly different trajectories, with cases A and B (Table 2) corresponding to Figs. 10a and b, respectively. For each of these two cases, flow visualization was performed at $Z/L=-0.84$ and $Z/L=-0.65$ (Table 2).

Case study		U^*	Z/L	$\zeta_Y(\%)$	A_Y^* at Z/L
A	A1	6.6	-0.65	0.45	0.32
	A2	6.6	-0.84	0.45	0.15
B	B1	6.6	-0.65	0.66	0.24
	B2	6.6	-0.84	0.66	0.11

Table 2 TEST CONDITIONS FOR FLOW VISUALIZATION.

An analysis of flow visualization images revealed that double roll up of the shear layers occurs in the near wake. A representative image shown in Fig. 12 suggests that the flow topology is similar to the 2P vortex shedding pattern [12] observed for VIV of one DOF circular cylinders. However, the downstream development of the wake vortices was found to depend significantly on the test conditions.

Cases A1 and A2: Based on the downstream evolution of the two co-rotating vortices shed each half cycle, two distinct types of wake development for case A1 are depicted in Figs. 13 and 14. An analysis of flow visualization videos and images showed that two counter-clock-wise (CCW) vortices, shed from the left hand side of the cylinder, merge within about four diameters downstream of the cylinder. This is illustrated in Fig. 13. However, occasionally, these vortices remain separated in the near wake (Fig. 14). Adopting the terminology introduced by Cerretelli and Williamson [27], vortex merging process can be broken into four stages, namely, first diffusive, convective, second diffusive, and merged diffusive stages. The merged vortex identified in Fig. 13 is representative of the last stage of vortex merging [27]. It should be noted that the clock-wise (CW) vortices shed on the right hand side of the cylinder have not been observe to merge in the near wake.

As the elevation is decreased along the span of the cylinder (case A2), the CCW as well as the CW vortices merge

within about ten diameters downstream of the cylinder. Comparing the results for cases A1 and A2 (compare e.g., Figs. 13 and 15), it can be seen that vortex merging occurs within a longer region at lower elevations. For case A2, the pattern of the merged co-rotating vortices is similar to the 2S vortex shedding pattern (Fig. 15).

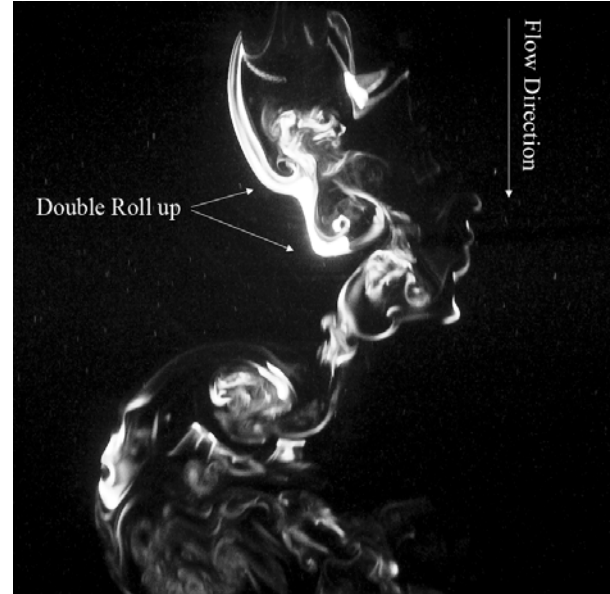


FIG. 12 FLOW VISUALIZATION OF THE DOUBLE ROLL UP OF SHEAR LAYERS FOR $U^*=6.6$, $Z/L=-0.65$, AND $\zeta_Y=0.45\%$.

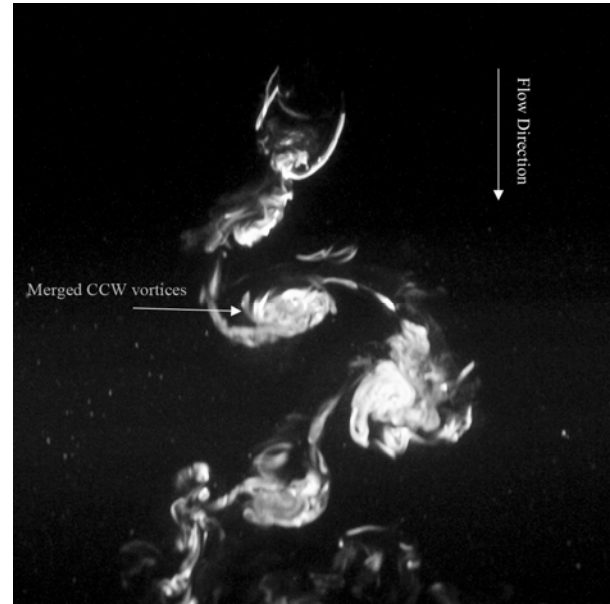


FIG. 13 VORTEX MERGING FOR CASE A1 ($U^*=6.6$, $Z/L=-0.65$, AND $\zeta_Y=0.45\%$).



FIG. 14 2P-LIKE SHEDDING PATTERN FOR CASE A1, ($U^*=6.6$, $Z/L=-0.65$, AND $\zeta_Y=0.45\%$).

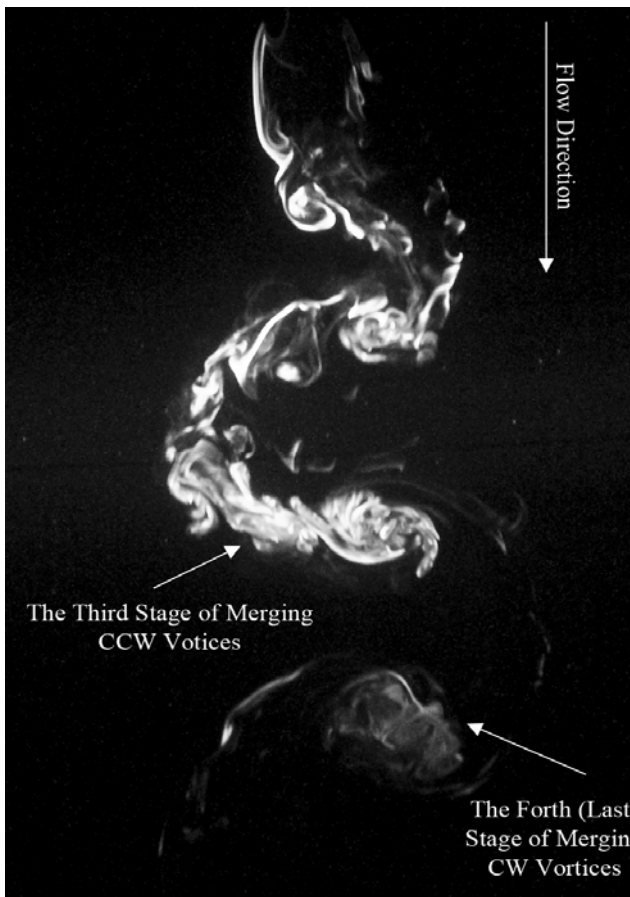


FIG. 15 FLOW VISUALIZATION OF CASE A2, ($U^*=6.6$, $Z/L=-0.84$, AND $\zeta_Y=0.45\%$).

Cases B1 and B2: At the higher elevation (case B1), a 2P vortex shedding pattern occurs (Fig. 16). In contrast, at the lower elevation (case B2), a vortex shedding pattern similar to that for case A2 (Fig. 15) was observed.



FIG. 16 FLOW VISUALIZATION FOR CASE B1 ($U^*=6.6$, $Z/L=-0.65$, AND $\zeta_Y=0.66\%$)

Analysis of vortex shedding patterns: Comparing the wake flow development at a constant U^* shows that changing the transverse damping ratio can affect the wake vortex shedding patterns. The shedding pattern is expected to depend primarily on the response of the structure [13]. For example, in the case of a one DOF uniform amplitude cylinder vibrations [13], varying the transverse amplitude of response can produce different shedding patterns at a given U^* (Fig. 17). Thus, the observed variation in the vortex shedding pattern between cases A1 and B1 is attributable to the associated changes in the amplitudes of response caused by the variation of the transverse damping ratio (Figs. 4 and 5). On the other hand, the attendant change in the transverse amplitude is not sufficient to affect vortex shedding patterns at lower elevations (cases A2 and B2).

It is of interest to investigate if wake vortex shedding patterns for two DOF linear amplitude cylinder vibrations can be predicted based on the results available for one DOF cylinders. In Fig.17, the current results pertaining to cases A1, A2, B1, and B2 (Table 2) are overlaid onto an updated Williamson-Roshko map from [13]. The map predicts a 2P vortex shedding pattern for cases A1 and B1. Indeed, the double roll up of the separated shear layer was observed for

these cases. However, unlike 2P shedding seen in the near wake for case B1 (Fig. 16), flow visualization shows frequent merging of CCW vortices for case A1 (Fig. 13). For the lower elevation, the map predicts an intermittent switching between the 2P and “non-synchronized” pattern for case A2 and the non-synchronized pattern for case B2. In contrast, for both cases, flow visualization reveals a transition from 2P to 2S vortex shedding pattern. The foregoing comparison suggests that the results pertaining to one DOF uniform amplitude VIV should not, in general, be extrapolated to the cases of two DOF linear amplitude VIV. A similar conclusion can be reached based on the results of Leong and Wei [23].

The present results show that the vortex shedding pattern can change along the span of the cylinder. Therefore, vortex dislocations, accompanied by complex vortex connections, are expected to occur along the span. Moreover, a simultaneous occurrence of synchronized and non-synchronized vortex shedding patterns at two different elevations, such as that predicted by the map in Fig. 17 for cases B1 and B2, is not possible since vortex lines cannot terminate in the fluid. Thus, at a given Reynolds number, a new, multidimensional map needs to be composed to predict vortex shedding patterns along the span of a cylindrical structure undergoing two DOF variable amplitude VIV.

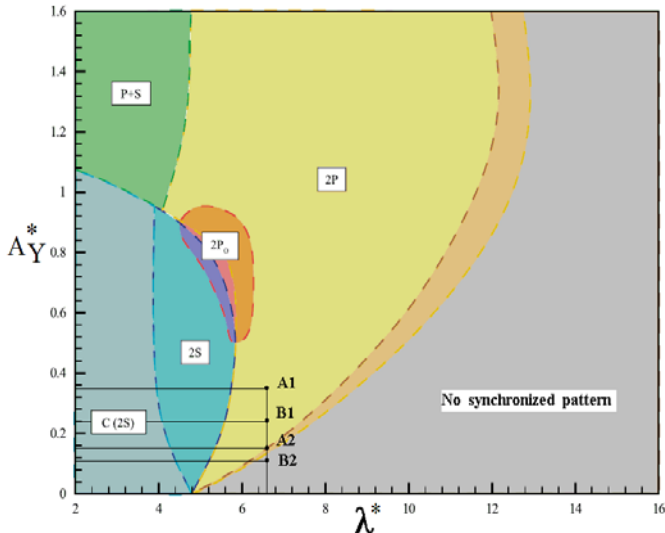


FIG. 17 COMPARISON OF CASES A AND B WITH THE RESULTS OF MORSE AND WILLIAMSON [13]. NOTE THAT $\lambda^* = U^*$ IN THE SYNCHRONIZATION REGION

4. CONCLUSIONS

The structural response and wake flow development of a two DOF pivoted cylinder with moderate mass ratio and high moment of inertia ratio have been investigated. Maintaining the Reynolds number constant throughout all of the experiments, the transverse damping ratio is shown to have a significant effect on the amplitude response. The spectral analysis of the transverse vibrations in the synchronization region shows a single peak centered at the natural frequency of the structure. In

contrast, multiple peaks centered at the Strouhal frequency, the natural frequency, and the harmonics of the natural frequency appear in the spectra pertaining to the non-synchronized region. In the synchronization region, the frequencies of transverse and streamwise vibrations lock onto the natural frequency, and the cylinder is observed to trace orbital trajectories. Such a response, common in some civil structures [25, 26], is different from Lisajous-type trajectories observed in previous studies [22, 23] and needs to be investigated further. The results presented reveal that, within the synchronization region, the phase angle between the transverse and streamwise vibrations is constant for a given U^* and ζ_y . When both the streamwise and transverse frequencies lock onto the natural frequency, the simple mathematical representation of the structural response is shown to predict orbiting motion similar to that observed experimentally.

For $U^* = 6.6$, the flow visualization results reveal a double roll up of shear layers in the formation region of the cylinder. However, it is shown that changing the transverse damping ratio affects the amplitude response, which can result in different vortex dynamics in the near wake. Specifically, vortex merging can occur in the near wake, resulting in a 2S-like pattern downstream. Also, for a given reduced velocity and transverse damping ratio, the variation of the vortex shedding pattern is observed along the span of the cylinder. A comparative analysis of the present findings and previous results for one DOF cylinders suggests that an updated map of vortex shedding is required to predict shedding patterns in the wake of a two DOF cylinder undergoing variable spanwise amplitude VIV.

ACKNOWLEDGMENTS

The authors gratefully acknowledge the Natural Sciences and Engineering Research Council of Canada (NSERC) and Ontario Centers of Excellence (OCE) for funding of this work.

REFERENCES

- [1] Huera-Huarte, F. J., and Bearman, P. W., 2009, “Wake structures and vortex-induced vibrations of a long flexible cylinder Part1: Dynamic response,” *J. Fluids Struct.*, **25**, pp. 969-990.
- [2] Dahl, J. M., Hover, F. S., and Triantafyllou, M. S., 2006, “Two-degree-of-freedom vortex-induced vibrations using a force assisted apparatus,” *J. Fluids Struct.*, **22**, pp. 807-818.
- [3] Carberry, J., Sheridan, J., Rockwell, D., 2005, “Controlled oscillations of a cylinder: forces and wake modes,” *J. Fluid Mech.*, **538**, pp. 31-69.
- [4] Feng, C. C., 1968, “The Measurement of Vortex-Induced Effects in Flow Past Stationary and Oscillating Circular and D-Section Cylinders,” MS thesis, University of British Columbia.
- [5] Skop, R. A., and Griffin, M., 1972, “A Model for the Vortex-Excited Resonant Response of Bluff Cylinders,” *J. Sound Vib.*, **27(2)**, pp. 225-233.

- [6] Griffin, O. M., Skop, R. A., and Koopmann, G. H., 1973, "The Vortex-Excited Resonant Vibrations of Circular Cylinders," 1973, **31(2)**, pp. 235-242.
- [7] Skop, R. A., and Griffin, O. M., 1975, "On a Theory for the Vortex-Excited Oscillations of Flexible Cylindrical Structures," *J. Sound Vib.*, **41(3)**, pp. 263-274.
- [8] Khalak, A., and Williamson, C. H. K., 1999, "Motions, Forces and Mode Transitions in Vortex-Induced Vibrations at Low Mass-Damping," *J. Fluids Struct.*, **13**, pp. 813-851.
- [9] Morse, T. L., and Williamson, C. H. K., 2006, "Employing Controlled Vibrations to Predict Fluid Forces on a Cylinder Undergoing Vortex-Induced Vibration," *J. Fluids Struct.*, **22**, pp. 877-884.
- [10] Morse, T. L., and Williamson, C. H. K., 2008, "The effect of end conditions on the vortex-induced vibration of cylinders," *J. Fluids Struct.*, **24**, pp. 1227-1239.
- [11] Williamson, C. H. K., and Govardhan, R., 2004, "Vortex-Induced Vibrations," *Annu. Rev. Fluid Mech.* **36**, pp. 413-455.
- [12] Williamson, C. H. K., and Roshko, A., 1988, "Vortex Formation in the Wake of an Oscillating Cylinder," *J. Fluids Struct.*, **2**, pp. 355-381.
- [13] Morse, T. L., and Williamson, C. H. K., 2009, "Fluid Forcing, Wake Modes, and Transitions for a Cylinder Undergoing Controlled Oscillations," *J. Fluids Struct.*, **25**, pp. 697-712.
- [14] Bearman, P. W., 1984, "Vortex shedding from oscillating bluff bodies," *Annu. Rev. Fluid Mech.* **16**, pp. 19-222.
- [15] Sarpkaya, T., 2004, "A Critical Review of the Intrinsic Nature of Vortex Induced Vibrations," *J. Fluids Struct.*, **19**, pp. 389-447.
- [16] Jauvtis, N., and Williamson, C. H. K., 2004, "The Effect of Two Degrees of Freedom on Vortex-Induced Vibration and at Low Mass and Damping," *J. Fluid Mech.*, **509**, pp. 23-62.
- [17] Jeon, D., and Gharib, M., 2001, "On Circular Cylinders Undergoing Two-Degree-of-Freedom Forced Motions," *J. Fluids Struct.*, **15**, pp. 533-541.
- [18] Gharib, M. R., 1999, "Vortex-Induced Vibration, Absence of Lock-in and Fluid Force Deduction," PH.D. , California Institute of Technology, Pasadena, CA.
- [19] Blevins, R. D., Coughran, C. S., 2009, "Experimental Investigation of Vortex Induced Vibration in One and Two Dimensions With Variable Mass, Damping, and Reynolds Number," *ASME, J. Fluids Eng.*, **131**, pp. 101202-7.
- [20] Sanchis, A., Saelevik, G., and Grue, J., 2008, "Two Degrees-of-Freedom Vortex-Induced Vibrations of a Spring Mounted Rigid Cylinder With Low Mass Ratio," *J. Fluids Struct.*, **24**, pp. 907-919.
- [21] Sarpkaya, T., 1995, "Hydrodynamic Damping, Flow-Induced Oscillations, and Biharmonic Response" *ASME J. Appl. Mech.*, **117**, pp. 232-238.
- [22] Flemming, F., Williamson, C. H. K., 2005, "Vortex-Induced Vibrations of a Pivoted Cylinder," *J. Fluid Mech.*, **522**, pp. 215-252.
- [23] Leong, C. M., and Wei, T., 2008, "Two-Degree-of-Freedom Vortex-Induced Vibration of a Pivoted Cylinder below Critical Mass Ratio," *Proc. R. Soc. A*, **464**, pp. 2907-2927.
- [24] Oniszcuk, Z., 2002, "Damped Vibration Analysis of a Two-Degree-of-Freedom Discrete System," *J. Sound Vib.*, **257(2)**, pp. 391-403.
- [25] Wardlaw, R. L., Cooper, K. R., Ko, R. G., and Watts, J. A., 1975, "Wind Tunnel and Analytical Investigations into the Aeroelastic Behavior of Bundled Conductors," In *Wind-Excited Vibrations of Structures*, Sockel, H. Springer-Verlag, Wien-New York, 1994, pp. 352-363.
- [26] So, R. M. C., Wang, X. Q., Xie, W. C., and Zhu, J., 2008, "Free-Stream Turbulence Effects on Vortex-Induced vibration and Flow-Induced Force of an Elastic Cylinder," *J. Fluids Struct.*, **24**, pp. 481-495.
- [27] Cerretelli, C., and Williamson, C. H. K., 2003, "The physical mechanism for vortex merging," *J. Fluid Mech.* **475**, 41-77.